

# A Morphological Approach to the Simulation of Forearm Motion

P. Fürnstahl<sup>1</sup>, A. Schweizer<sup>2</sup>, L. Nagy<sup>2</sup>, G. Székely<sup>1</sup>, M. Harders<sup>1</sup>

<sup>1</sup>Computer Vision Laboratory, ETH Zurich, Zurich, Switzerland

<sup>2</sup>Department of Orthopedic Surgery, Balgrist University Hospital, Zurich, Switzerland

**Abstract**—Computer-based simulations support surgeons in preoperative planning of osteotomy and assessing the improvement of the forearm motion. To this end, an in-silico model of patient-specific forearm kinematics is required. In this paper we introduce a motion model of the forearm which is based on a patient's joint morphology, the form and shape of the joints. The morphology of the articulations is represented by 3-dimensional splines. In this way the gliding motion of the articulations is expressed analytically in a closed-form. Our algorithm was designed to work with available clinical planning data and requires minimal user interaction. This allows an integration in computer-aided planning systems that are operated by surgeons. The accuracy of the simulation results is verified via cadaver experiments.

**Index Terms**—forearm, kinematic, pro- and supination

## I. INTRODUCTION

Posttraumatic forearm malunions can cause pathological bone impingements between radius and ulna, as well as increased tension in involved ligaments. This results in an impairment of the forearm range of motion (ROM) or pain in the distal radioulnar joint (DRUJ) [1]. Corrective osteotomy is the preferred treatment to improve the overall ROM and to alleviate pain. In current clinical planning the contralateral healthy side is used as a reference. However, important side to side variabilities exist in the healthy population [2], [3]. In order to improve the reliability and outcome of this surgical intervention, computer-based planning, independent of the healthy side, is of great clinical interest [1]. Therefore, the goal of our current research is to develop a planning system to virtually assess the outcome of surgical corrections and to simulate the resultant ROM. One of the central elements of such a tool is the correct simulation of the forearm motion. In this paper we present a new kinematic model able to accurately reproduce the forearm motion from supination (palm up) to pronation (palm down).

Several developments related to our work have been carried out in the past. Fick [4] published the first motion model of the forearm in 1904. In his method the ulna was fixed with respect to the humerus and the pro-/supination was defined by a rotation of the radius around a constant axis. However, this assumption resulted in an unrealistic tilt of the wrist.

Based on MRI findings, more comprehensive kinematic models were developed that include the motion of the ulna [5], [6]. Kasten, Weinberg *et al.* introduced a surrogate mechanism for the pro-/supination where the influence of

joints were taken into account by a simplified mechanical analogy [6], [7]. The fitting of kinematics to patient-specific anatomy was manually performed by measuring geometric attributes from radiographs, for instance bone lengths. It was possible to predict rotational impairments based on angular deformities using this model. Kecskeméthy and Weinberg [8] later extended this basic model by introducing virtual springs to also incorporate elastic components, for instance ligaments.

In addition to this, complex musculoskeletal models of the upper limb have been developed, often including the simulation of soft tissue [9], [10]. However, in [10] the simulation of the pro-/supination is simplified by neglecting the swaying angle of the ulna. Moreover, the usability of these musculoskeletal systems for surgical planning is often limited, since patient-specific anatomy cannot easily be included [9].

The key concept of our approach, and the main difference to previously published work, is to directly simulate the forearm motion based on patient-specific joint morphology instead of a physically based model that is fit to the patient's data. We assume that the bone motion is mainly dictated by the shape of the interacting joint surfaces. Therefore, 3-d splines are determined based on patient morphology, which capture the gliding motion in the DRUJ and the evasive ulna movement. An additional advantage of our approach is that already two computed tomography (CT) scans of the forearm, in full pro- and supination respectively, provide sufficient data for a reasonably accurate motion prediction.

The accuracy of the simulation results is verified via a cadaver arm study. The forearm motion of two cadaver specimens was captured in discrete steps by CT and resulting segmented 3-d bone models are used as ground truth.

## II. METHODOLOGY

During pro-/supination the radius performs a fixed-point rotation with respect to the humerus. The center of rotation is located in the proximal radius head. Distally, the radius head rotates around the ulna while both bones are pressed together by ligaments in the DRUJ. Correspondingly, the distal ulna head glides in the sigmoid notch of the radius from a volar proximal to a dorsal distal position as the forearm moves from supination to pronation. Therefore, the rotation of the radius occurs around a variable screw axis. As a consequence, the ulna has to perform a lateral swaying and a small axial sliding with respect to the humerus in order

This work has been supported by the Swiss National Science Foundation

to avoid tilting of the wrist and ensure parallelism between the hand and the forearm [8].

Our proposed kinematic model is derived based on the fundamental characteristics of this movement and by additionally including joint morphology. In order to transform the complex motion of radius and ulna into a simpler model, the bone movement is expressed with respect to the ulna instead of using the humerus as the reference. In this way only the transformation of the radius has to be considered but the actual motion between radius and ulna is not altered. Subsequently, the kinematics in the distal and proximal articulations are analyzed and combined to calculate a rigid body transformation for a given pro-/supination angle  $\varphi$ . Finally, the parameters of our model are optimized to achieve best fitting with the patient's CT data.

In order to set up the kinematic model, at least two CT scans of the proximal and distal articulations are required, in full supination and full pronation, respectively. The bone geometry, represented as triangular meshes, is acquired using an in-house developed segmentation algorithm based on graph cuts [11], [12]. Segmentation and mesh generation can be performed in less than one minute with minimal user interaction. Thereafter, the resulting meshes are transformed to an ulna coordinate system by registering the ulnae with an iterative closest point (ICP) algorithm [13] as depicted in Figure 1 (a).

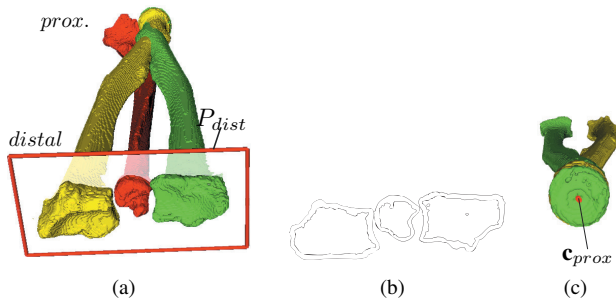


Fig. 1. Anatomical features used for the motion simulation are extracted from two CT scans of the forearm in full pronation and full supination, respectively. (a) Radius models in pronation (left) and supination (right) relative to the ulna (middle), (b) 2-d contours are interactively rendered according to  $P_{dist}$ , (c) The proximal rotation center  $\mathbf{c}_{prox}$  with respect to the humerus is automatically detected. Points with marginal positional variation over the acquired CT scans are marked red.

### A. Distal Movement

Distally, the pro-/supination can be rendered in ulna coordinates by gliding the radius sigmoid notch around the virtually fixed ulna. In our model the movement is restricted to a plane  $P_{dist}$  perpendicular to the ulna length axis, since the parallelism constraint has to be fulfilled. The position of  $P_{dist}$  on the ulna length axis is defined by the user in such a way that the 2-d contours of the radial sigmoid notches in the data sets of the pronated and supinated radius are both most pronounced. To this end, the mesh vertices are clipped by slicing the mesh with  $P_{dist}$  as shown in Figure 1 (a). A tool is provided to the user that interactively renders the contours of the sliced meshes while the plane is moved along the axis

as demonstrated in Figure 1 (b). This allows to easily define the location of  $P_{dist}$  along the bone axis. In the next step the parts of the contours are identified that are involved in the sliding motion according to Figure 2. The relevant curves are determined by finding first guesses of the start- and end-points on the ulna and radius outlines in FS. The start-point  $\mathbf{u}_0$  on the ulna is set to the contour-point that is closest to the radius in supination. End-point  $\mathbf{u}_1$  is defined by the point that is closest to the pronated radius. The corresponding points on the radii are  $\mathbf{r}_0$  and  $\mathbf{r}'_1$ , respectively. In order to define the end-point  $\mathbf{r}_1$  on the supinated radius, the transformation of the contour from pronation to supination is calculated by 2-d ICP registration. This allows to transform  $\mathbf{r}'_1$  to  $\mathbf{r}_1$ . Additionally, the required ROM  $\varphi_{max}$  from supination to pronation can be obtained, since it corresponds to the rotation of the registration.

The calculation of  $\varphi_{max}$ , as well as the identification of the start- and end-points is performed automatically. However, some minor inaccuracies can still exist, which will be corrected in an optimization step as described below. In order to extend the search space of this optimization, each determined curve is elongated by extending the start- and end-points along the bone contours by a user-defined value (*i.e.* 4 mm). In 2-d this can be easily done by replacing the current start- or end-points with their neighbors that elongate the curves until the threshold is reached. Finally, the contour fragments of the radius and the ulna are converted to parametric bicubic 3-d splines  $\Gamma_{dist}^R$  and  $\Gamma_{dist}^U$ , respectively. These splines are defined by determining all 2-d contour points lying between the corresponding start- and end-point using Dijkstra's shortest path algorithm. The remaining third coordinate for each point is derived from the plane equation.

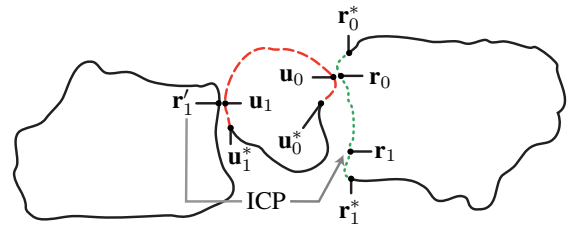


Fig. 2. Extracted 2-d contours obtained from two CT data sets of the distal radius in full pronation (left) and full supination (right). The ulna contour is shown in the middle. Points  $\mathbf{r}_0/\mathbf{r}_1$  and  $\mathbf{u}_0/\mathbf{u}_1$  define the gliding curves on the radius (dotted) and the ulna (dashed), respectively. Points denoted with an asterisk correspond to start-/end-points after the mentioned curve elongation.

### B. Proximal Movement

First, the radius rotation center  $\mathbf{c}_{prox}$  of the fixed-point rotation with respect to the humerus is automatically determined. To this end the radii of the data sets, used for the motion generation, are registered to find corresponding mesh points. Thereafter, the transformations of the radii are described relative to the humerus in order to determine the fixed point as illustrated in Figure 1 (c). The humerus coordinate system is obtained by ICP registration of the humeri

models extracted from the acquired CT scans in the pro-/supination positions. The fixed-point rotation center  $\mathbf{c}_{prox}$  is finally located by choosing the most proximal point with marginal positional variation over the different positions, since it is fixed during rotation relative to the humerus.

In ulna coordinates the proximal rotation center  $\mathbf{c}_{prox}$  is no longer fixed and has to perform the inverse evasive motion of the ulna. The evasive motion of the ulna is obtained by registering the ulnae using humerus coordinates. Starting from supination the final movement of the proximal radius is approximated according to the measured inverse motion of the ulna. A 3-d spline  $\Gamma_{prox}^R$  is generated that correspondingly interpolates the transformation of  $\mathbf{c}_{prox}$  in ulna coordinates. In case of two acquired positions, the swaying movement is linearly interpolated from full supination to full pronation.

### C. Simulation of Motion

For the simulation of the pro-/supination the distal and proximal movements are combined in a rigid body transform for the radius. Given the desired angle  $\varphi \leq \varphi_{max}$ , the appropriate  $4 \times 4$  transformation matrix is calculated relative to the initial position in FS ( $\varphi = 0$ ). At least three 3-d point pairs  $(\mathbf{p}_i, \mathbf{q}_i)$  are required to compute this matrix, where  $\mathbf{p}_i$  and  $\mathbf{q}_i$  denote points on the radius in the initial and final position, respectively. The resultant transformation optimally maps each  $\mathbf{p}_i$  to  $\mathbf{q}_i$  in a least squares sense and thus the radius is moved to the desired position. The three point pairs, two from the distal articulation and one from the proximal joint, are defined as follows.

The first pair  $(\mathbf{p}_0, \mathbf{q}_0)$  reflects the gliding motion of the radius in the DRUJ.  $\mathbf{p}_0$  is obtained from the parameterized radius spline  $\Gamma_{dist}^R(t)$ :

$$\mathbf{p}_0 = \Gamma_{dist}^R \left( t_{r_0} + \frac{\varphi}{\varphi_{max}} (t_{r_1} - t_{r_0}) \right),$$

where  $t_{r_0}$  and  $t_{r_1}$  represent the parameterized start- and end-points of  $\Gamma_{dist}^R$ . Since the distal radius glides around the ulna head,  $\mathbf{q}_0$  can be obtained from the ulna spline  $\Gamma_{dist}^U(t)$  as

$$\mathbf{q}_0 = \Gamma_{dist}^U \left( t_{u_0} + \frac{\varphi}{\varphi_{max}} (t_{u_1} - t_{u_0}) \right) + \Delta \cdot \mathbf{n}_t,$$

where  $\mathbf{n}_t$  is the spline normal at  $t$ .  $t_{u_0}$  and  $t_{u_1}$  denote the start and end parameters of  $\Gamma_{dist}^U$ . A geometrical interpretation is given in Figure 3. The additional parameter  $\Delta$  represents the distance between radius and ulna head in the DRUJ, since no direct contact between bones occurs in the articulation due to cartilage (this can also be observed in CT images as shown in Figure 3 (a)). The parameters are initialized to  $\Delta = 0.25$ ,  $t_{r_0} = 0.0$ ,  $t_{r_1} = 1.0$ ,  $t_{u_0} = 0.0$ , and  $t_{u_1} = 1.0$ , however, the final values will be determined in an optimization step.

The second point pair  $(\mathbf{p}_1, \mathbf{q}_1)$  encodes the rotation of the distal radius head and is also constrained to lie on plane  $P_{dist}$  in order to guarantee parallelism between forearm and wrist. Let  $\mathbf{p}_1 = \mathbf{p}_0 + \mathbf{v}$  where  $\mathbf{v}$  is an arbitrary direction vector lying on  $P_{dist}$  (i.e.  $(0, 1)$ ). Vector  $\mathbf{v}$  is shown as an arrow in

Figure 3 (b). In the pro-/supination position  $\varphi$ , vector  $\mathbf{v}$  has to be rotated by  $\varphi$ , according to the radius head. As previously shown,  $\mathbf{p}_0$  is transformed to  $\mathbf{q}_0$ . Therefore,  $\mathbf{q}_1 = \mathbf{q}_0 + \mathbf{R}_\varphi \mathbf{v}$  where  $\mathbf{R}_\varphi$  describes the rotation by  $\varphi$  degrees.

The points  $(\mathbf{p}_2, \mathbf{q}_2)$  denotes the evasive movement of the proximal radius head relative to the ulna. Point  $\mathbf{p}_2$  is set to the beginning of the proximal spline  $\Gamma_{prox}^R(0)$ . During pro-/supination  $\mathbf{p}_2$  is transformed to  $\mathbf{q}_2 = \Gamma_{prox}^R(\varphi/\varphi_{max})$ .

The absolute orientation problem [14] is finally solved to determine the radius transformation matrix based on the three point pairs and the given pro-/supination angle  $\varphi$ . In order to achieve a best possible fit to the acquired CT data, a non-linear optimization [15], based on Sequential Quadratic Programming, is applied to determine the values for the parameter vector ( $0 \leq \Delta \leq 0.5$ ,  $t_{r_0} \geq 0$ ,  $t_{r_1} \leq 1$ ,  $t_{u_0} \geq 0$ ,  $t_{u_1} \leq 1$ ). The objective function is defined as the squared distance between simulated and measured mesh points for coincident  $\varphi$ . The input data are forearm scans at different rotational positions, the minimum set being that of full supination and full pronation.

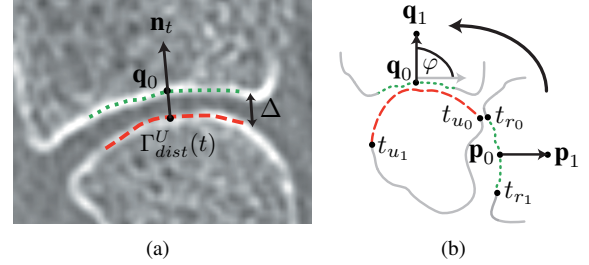


Fig. 3. Motion simulation in the DRUJ. Radius spline  $\Gamma_{dist}^R$  is marked dotted and ulna spline  $\Gamma_{dist}^U$  dashed, respectively. (a) Distance  $\Delta$  between bones has to be considered due to cartilage, (b) Generation of the gliding motion for  $\varphi = 90^\circ$

## III. RESULTS

We carried out cadaver experiments, using two fresh-frozen cadaveric arm specimens, to examine the accuracy of our approach. The study was approved by the local ethics committee of the Balgrist University Hospital. The experimental setup is shown in Figure 4. The humerus was rigidly mounted on a custom built frame using two Schanz' screws. The distal ulna was unicortically fixed with a carbon-fibre rod in such a way that the evasive movement was not limited. Two carbon-fibre rods were inserted in the radial styloid to allow external rotation of the radius in order to simulate the pro-/supination. CT scans were performed in mechanically controlled  $10^\circ$  steps from full supination to full pronation. A Philips Brilliance 40 CT scanner was used for data acquisition with an in-plane resolution of  $0.48 \times 0.48$  mm. The slice thickness/spacing was  $0.66/0.5$  mm and  $1/0.5$  mm in study 1 and study 2, respectively. Based on these CT data, 3-d models of all rotations were generated using our segmentation method [11].

For accuracy evaluation two different error metrics were applied, both based on the distance between the simulated forearm position and the corresponding mesh obtained from

the cadaver experiments. Measure  $\epsilon_1$  represents the average closest point distance between mesh points in simulated and measured position. A small distance error is crucial for a planning tool in order to detect possible bone impingements. We achieved an average error over all measured positions of  $\epsilon_1 = 0.44 \pm 0.19$  mm in study 1 and  $\epsilon_1 = 0.48 \pm 0.21$  mm in study 2, respectively. Note that positions full pronation and full supination were excluded from the evaluation since the meshes were used to setup the algorithm. Error measure  $\epsilon_2$  is defined by the average distance between *corresponding* mesh points, obtained by registration, in simulated and measured positions and is, therefore, more sensitive to orientation errors. The average error in study 1 was  $\epsilon_2 = 0.65 \pm 0.44$  mm and in study 2  $\epsilon_2 = 0.98 \pm 0.51$  mm, respectively. More details are given in Figure 5. The Figure also shows the effect on accuracy when including additional arm positions in the optimization.



Fig. 4. Experimental setup of the cadaver study.

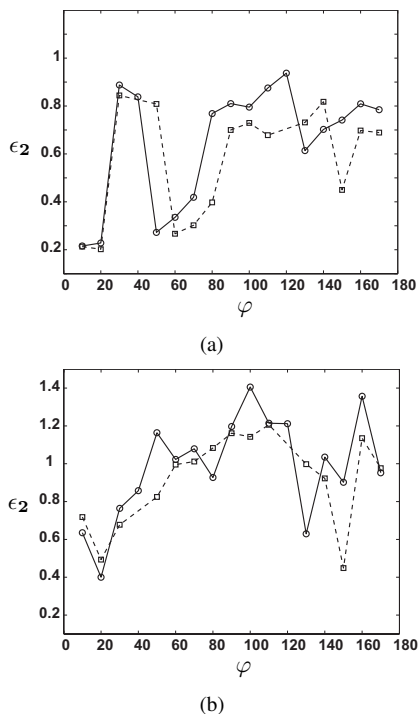


Fig. 5. Evaluation of error  $\epsilon_2$  (mm) in cadaver study 1 (a) and study 2 (b) for a given pro/supination angle  $\varphi$ . For optimization either two ( $\varphi = 0$ ,  $\varphi = 180$ ) or four positions ( $\varphi = 0$ ,  $\varphi = 40$ ,  $\varphi = 120$ ,  $\varphi = 180$ ) were used, denoted by circles (solid line) and squares (dashed line), respectively. Positions used for optimization were excluded from the evaluation.

#### IV. CONCLUSION AND OUTLOOK

In this paper we have presented an approach for the simulation of the forearm motion. Instead of solely fitting a model to the patient's data, we generate the motion based on the shape of the DRUJ. CT scans only of a patient's arm in full pronation and full supination appeared to be sufficient for determining forearm motion. Moreover, the initialization of the algorithm requires only minimal user interaction. This allows to easily incorporate our method in the current clinical planning practice. For future work we plan to use the kinematic model for the simulation of impaired motion caused by malunited bones to provide surgeons with a comprehensive virtual osteotomy planning tool.

#### REFERENCES

- [1] L. Nagy, L. Jankauskas, and C. Dumont, "Correction of forearm malunion guided by the preoperative complaint," *Clin Orthop Relat Res*, vol. 466, no. 6, pp. 1419–1428, June 2008.
- [2] R. R. Bindra, R. J. Cole, K. Yamaguchi, B. A. Evanoff, T. K. Pilgram, G. L. A., and G. R. H., "Quantification of the radial torsion angle with computerized tomography in cadaver specimens," *J Bone Joint Surg Am.*, vol. 79, no. 6, pp. 833–837, 1997.
- [3] C. E. Dumont, L. Nagy, D. Ziegler, and P. C. W., "Fluoroscopic and magnetic resonance cross-sectional imaging assessments of radial and ulnar torsion profiles in volunteers," *The Journal of Hand Surgery*, vol. 32, no. 4, pp. 501–509, April 2007.
- [4] R. Fick, *Handbuch der Anatomie und der Mechanik unter Berücksichtigung der bewegenden Muskeln*. Fischer Verlag, 1904.
- [5] T. Nakamura, Y. Yabe, Y. Horiuchi, and N. Yamazaki, "In vivo motion analysis of forearm rotation utilizing magnetic resonance imaging," *Clin Biomech*, vol. 14, no. 5, pp. 315–320, June 1999.
- [6] A. Weinberg, I. T. Pietsch, M. B. Helm, J. Hesselbach, and H. Tscherne, "A new kinematic model of pro- and supination of the human forearm," *J Biomech*, vol. 33, no. 4, pp. 487–491, April 2000.
- [7] P. Kasten, M. Krefft, J. Hesselbach, and A. Weinberg, "Computer simulation of forearm rotation in angular deformities: a new therapeutic approach," *Injury*, vol. 33, no. 9, pp. 807–813, November 2002.
- [8] A. Kecskeméthy and A. Weinberg, "An improved elasto-kinematic model of the human forearm for biofidelic medical diagnosis," *Multi-body System Dynamics*, vol. 14, no. 1, pp. 1–21, August 2005.
- [9] K. Holzbaur, W. Murray, and S. Delp, "A model of the upper extremity for simulating musculoskeletal surgery and analyzing neuromuscular control," *Ann Biomed Eng*, vol. 33, no. 6, pp. 829–840, June 2005.
- [10] D. Blana, J. G. Hincapie, E. K. Chadwick, and R. F. Kirsch, "A musculoskeletal model of the upper extremity for use in the development of neuroprosthetic systems," *J Biomech*, vol. 41, no. 8, pp. 1714–1721, 2008.
- [11] P. Fürnstahl, T. Fuchs, A. Schweizer, L. Nagy, G. Székely, and M. Harders, "Automatic and robust forearm segmentation using graph cuts," in *Biomedical Imaging: ISBI 2008*. Paris, France: IEEE, May 2008, pp. 77–80.
- [12] M. Harders, A. Barlit, C. Gerber, J. Hodler, and G. Székely, "An optimized surgical planning environment for complex proximal humerus fractures," in *MICCAI Workshop on Interaction in Medical Image Analysis and Visualization*, 2007.
- [13] Y. Chen and G. Medioni, "Object modelling by registration of multiple range images," *Image and Vision Computing*, vol. 10, no. 3, pp. 145–155, 1992.
- [14] B. K. Horn, "Closed-form solution of absolute orientation using unit quaternions," *J Opt Soc Am A*, vol. 4, pp. 629–642, April 1987.
- [15] C. Lawrence, J. L. Zhou, and T. A. L., "Users guide for cfsqp version 2.5," Tech. Rep., 1997.